Conference on Modelling Fluid Flow (CMFF'22)
The 18th International Conference on Fluid Flow Technologies
Budapest, Hungary, August 30 -September 2, 2022

FLUID DYNAMICS IN A COUNTERCURRENT BUBBLE COLUMN: EXPERIMENTS AND SIMULATIONS

Péter KOVÁTS[1*], Katharina ZÄHRINGER[1], Haris KHAN[2], Roland RZEHAK[2], and Dominique THÉVENIN[1]

[1] Laboratory of Fluid Dynamics and Technical Flows, Otto-von-Guericke-Universität Magdeburg. Universitätsplatz 2, D-39106 Magdeburg, Germany. Tel.: +49 391 - 67 58654, Fax: +49 391 - 67 52840
*E-mail: peter.kovats@ovgu.de
[2] Helmholtz-Zentrum Dresden – Rossendorf, Institute of Fluid Dynamics, Bautzner Landstrasse 400, D-01328 Dresden, Germany

ABSTRACT

Flows in bubble columns are used in many applications in diverse branches of engineering. Moreover, they provide a simple configuration to study fundamental aspects of multiphase flows. Additional co- or countercurrent liquid flow is often used to adjust the residence-time of the bubbles, which is particularly important when mass-transfer occurs. The present contribution reports the initial stage of a joint experimental and numerical effort to understand such flows and to provide models that allow to predict them. To this end, experiments are carried out in a laboratory-scale bubble column and compared with corresponding simulations based on the Euler-Euler framework.

Keywords: bubble column reactor, dispersed two-phase flow, countercurrent flow, shadow imaging, PIV, CFD, Euler-Euler simulation

NOMENCLATURE

a	[mm]	major semi-axis
b	[mm]	minor semi-axis
d_b	[mm]	mean bubble size
d_h	[m]	hydraulic diameter
ESD	[mm]	equivalent sphere diameter
Q_g	[l/h]	gas volume flow rate
Q_l	[l/min]	liquid volume flow rate
v_b	[m/s]	bubble velocity
V_b	[m^3]	volume of the bubble spheroid
v_l	[m/s]	liquid velocity
v_y	[m/s]	vertical liquid velocity
α_G	[-]	gas fraction
μ	[$Pa\,s$]	liquid dynamic viscosity
ρ	[kg/m^3]	liquid density
Re	[-]	Reynolds number

1. INTRODUCTION

Bubble column reactors are simple multiphase contactors, where a gas phase is dispersed in a continuous liquid phase. Since they have no moving parts, the operation and maintenance of these reactors is simple. Bubble columns are widely used in chemical, biochemical and petrochemical industries. However e.g. in water and wastewater treatment, countercurrent flow of liquid and gas is applied to increase residence time and gas holdup as well as to enhance mixing and mass transfer.

Besides expensive experiments, multiphase CFD simulation is a smart tool in process engineering to study new reactor designs and scale them up from laboratory to industrial scale [1]. However, to reach industrial scales, the Euler-Euler framework has to be applied for multiphase flow, which heavily relies on modelling unresolved small-scale phenomena (e.g. [2-4] and references therein). Therefore, such simulations have to be validated with experimental data [5].

For these reasons, experiments are carried out in a laboratory-scale bubble column under counter-current flow conditions. For the same setup, Euler-Euler multiphase CFD simulations are performed using a set of closure relations that was extensively validated for co-current flow in pipes and bubble columns in previous works [6, 7]. A monodisperse approximation in the simulations is made feasible by generating bubble swarms of almost uniform size with seven small nozzles in the experiments so that the complexity of modelling bubble breakup and coalescence can be avoided. By comparing the simulation results with the experimental measurements, the validity of the closure models can be established also for counter-current flows. This is a prerequisite for later planned joint investigations of mass transfer phenomena.

Two experiments were performed for several flow conditions with different measurement set-ups. The first investigates properties of the dispersed gas phase such as bubble diameter and bubble velocities by shadow imaging. The second characterizes the

flow of the continuous liquid phase. These data can then be evaluated further to derive correlations for modelling of such two-phase flows. Another objective of these experimental measurements is to provide experimental data for the validation of numerical models. Some preliminary CFD simulation results are also presented in this paper.

2. EXPERIMENTAL SET-UP

To characterize the gas and liquid flow in the bubble column, two different optical measurement methods have been applied, see e.g. [8, 9]. First, the characteristics of the bubbles, such as bubble diameter, velocity, shape or position were measured with shadow imaging. This technique is based on shadow particle recognition combined with Particle Tracking Velocimetry (PTV) to measure the velocity of the bubbles as described in detail in [9]. Then, for the liquid phase, Particle Image Velocimetry (PIV) was used to examine the surrounding hydrodynamics.

Bubble column reactor

A laboratory-scale bubble column with a square cross section of 0.1 x 0.1 m^2 was employed for both experiments (Figure 1). The bubble column was made from acrylic glass and it was especially designed for optical measurements. It consist of 6 main parts: two 0.5 m long inlet (Figure 1, a 1) and outlet (Figure 1, a 2) sections, the water inlet on top (Figure 1, a 3) through four 1" pipes, a 2 m tall acrylic pipe on top of the column with an inner diameter of 0.04 m for gas ventilation (Figure 1, a 4), the 1 m long effective measurement section (Figure 1, a 5) and an interchangeable gas distributor (Figure 1, a 6). In this gas distributor, seven nozzles were mounted in-line, with 12.5 mm equal spacing. The interchangeable design allows the use of different nozzle materials and diameters. In the present study, stainless steel nozzles were applied, with an inner diameter of 0.18 mm. The nozzles were separately connected to seven magnetic valves (Type 6712, Bürkert), which were supplied by a mass flow controller (F-201CV, Bronkhorst) and the pressurized air pipeline.

In order to avoid pulsations induced by a pump, the countercurrent water flow was driven by gravity from an upper water reservoir situated about 4 m above the bottom water reservoir (Figure 1, a 7). This set-up allows a maximum water flow rate of Q_l=55.5 l/min, which corresponds to a Reynolds-number of Re=9000 inside the bubble column. The Reynolds number is defined as $Re=(\rho \cdot v_l \cdot d_h)/\mu$, where ρ is the liquid density, v_l is the liquid velocity, d_h is the hydraulic diameter of the column and μ is the dynamic viscosity of the liquid. The top reservoir was filled with de-ionised water. All the measurements were made at atmospheric pressure and room temperature (20°C). The experimental flow conditions are summarized in Table 1. Shadow imaging measurements were carried out at 2, 6 and 10 l/h air flow rates, while PIV measurements were performed just at 6 and 10 l/h gas flow rates.

Table 1. Experimental conditions.

	Re	Q_g [l/h]	Q_l [l/min]
1	100	2; 6; 10	0.6
2	500	2; 6; 10	3.1
3	1800	2; 6; 10	11.1
4	5000	2; 6; 10	30.8
5	9000	2; 6; 10	55.5

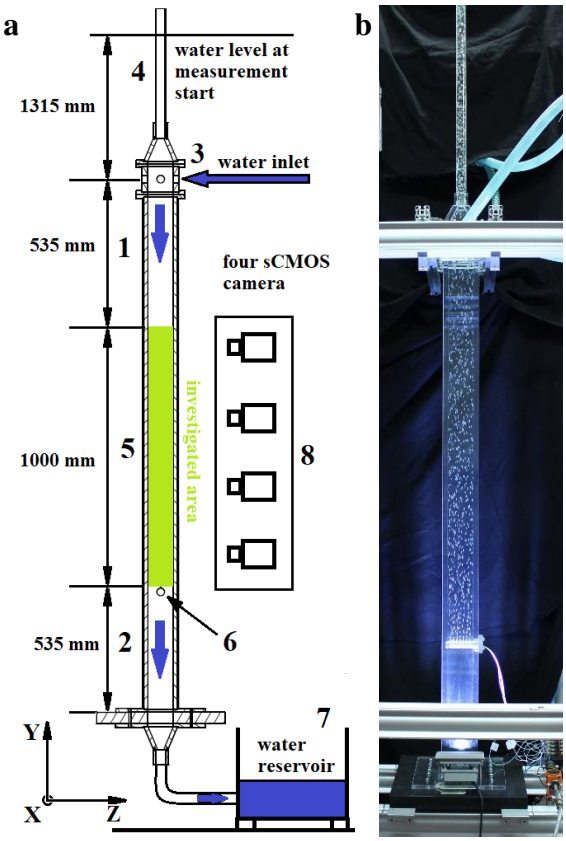

Figure 1. Experimental set-up (a) and photograph of the bubble column (b).

Shadow imaging set-up

For the shadow imaging measurements, four Imager sCMOS cameras (LaVision, (Figure 1, a 8)) were applied with a 2560 x 2160 pixels resolution and 80 Hz frame rate. The cameras were equipped with Nikon AF Nikkor 50 mm lenses. They were focused on the centre of the investigated column volume and the bubbles were, due to the depth of field, identified in a 33 mm thick region. To illuminate the measurement area and generate bubble shadows, 8 high-power COB LEDs (Luminus CXM-32) with an overall nominal power of 1120W were used. Because of the high illumination intensity and for the sake of a homogenous background illumination, the light was

diffused on white drawing paper. 3x1000 images were acquired with a frame rate of 80 Hz at each investigated condition. The experimental images were recorded and processed with the software DaVis (LaVision). Further post-processing steps were made in Matlab.

PIV set-up

For the PIV measurements, the same camera set-up was used as before for the shadow imaging, but in this set-up the cameras were equipped with band-pass filters (590 nm, 50 nm FWHM) to record only the fluorescence signal of the Rhodamin B doped polymethyl methacrylate (PMMA) seeding particles (mean diameter: 1-20 μm). These particles were excited by a double-pulse Nd:YAG laser (Quantel Evergreen) at 532nm. The laser beam was divided into two beams with a 50-50% mirror and these two beams were then expanded by two light sheet optics placed above each other, to illuminate the whole 1 m measurement section. The geometrical positions were calibrated with a 3D calibration target over the whole measurement section for both measurement methods. Overall, 4000 experimental images were acquired with 5 Hz in double frame mode for each investigated condition. The delay time between the two frames was 11 ms. From the recorded double-frame images, flow fields were calculated in DaVis. For the vector calculation, a cross-correlation (multi-pass, decreasing size) PIV algorithm was used with an interrogation window size from 64x64 pixels to 32x32 pixels, with 50% overlap. To remove false vectors and refine the vector field, especially in the vicinity and shadows of the bubbles, a median filter was applied.

3. SIMULATION SET-UP

Multiphase CFD simulations of the experiments are performed by applying the Euler-Euler framework with a set of closure relations that was extensively validated in previous works for various different geometries, including pipes, columns, and stirred tanks (e.g. [6, 7] and references therein). Concerning momentum transfer between the phases, closure comprises drag, shear-lift, wall-lift, virtual mass and turbulent dispersion forces, with models listed in Table 2. Turbulence in the liquid phase is described by a k-ω SST model (Menter [10]) with additional source terms for the bubble induced turbulence (Ma et al. [11]). In accordance with the experiments, a monodisperse approximation for the bubble size prescribing the experimentally determined mean value is suitable. The simulations are run in the open-source code OpenFOAM v8 with an add-on developed at HZDR [12].

Table 2. Summary of bubble force correlations.

force	**reference**
drag	Ishii [13]
shear lift	Tomiyama et al. [14]
wall lift	Hosokawa et al. [15]
turbulent dispersion	Burns et al. [16]
virtual mass	constant coefficient C_{VM} = ½

The computational domain consists of the 1 m long effective measurement section (Figure 1, a 5) together with the two 0.5 m long inlet (Figure 1, a 1) and outlet (Figure 1, a 2) sections, i.e. it is a 2 m high cuboid 0.1 x 0.1 m^2 cross section. On the side walls a no-slip condition is imposed for the liquid phase and a free-slip condition on the gas phase. Each nozzle is modelled by an individual patch through which the gas enters with a uniform velocity profile such that the total experimental flow rate is split evenly between the 7 nozzles. At the bottom of the column, a uniform flow with an outflow rate corresponding to the experiment is prescribed. At the top of the column the pressure is fixed. Since the area of observation extends only 1 m upwards from the nozzles, the effect of the imposed conditions at the column bottom and top can be expected to be small.

4. RESULTS

Shadowgraphy

The three series of 1000 acquired images were processed in DaVis to collect the parameters of each recognized bubble, like bubble major and minor axis, and velocity. The further data processing has been done in Matlab. First of all, from the major and minor axes of the bubbles the Equivalent Sphere Diameter (*ESD*) was calculated:

$$ESD = \sqrt[3]{\frac{3V_B}{4\pi}} \cdot 2\,, \qquad (1)$$

$$V_B = \frac{4}{3}\pi a^2 b, \qquad (2)$$

where V_B is the volume of the spheroid, a is the major semi-axis, and b is the minor semi- axis. For the further data evaluation, these bubble diameters were used. In the next step, the investigated domain (100x33x1000 mm^3) was divided into 5x5 mm^2 cells in which mean bubble diameters and velocities were calculated over all 3000 images. From these data, global mean parameters were calculated for each investigated condition, which are represented in Table 3. The results show that with increasing gas volume flow, the bubble size is increasing, as well as with an increasing countercurrent liquid flow. In contrast, the bubble velocity is decreasing with an increasing bubble size and it evidently decreases with an increasing countercurrent liquid

flow. Also a slight growth can be found in bubble velocities with increasing gas flow rate.

Table 3. Global mean results of bubble diameters and velocities.

Q_g [l/h]	Q_l[l/min]	*ESD* [mm]	v_b [m/s]
2	0.6	3.28	0.295
2	3.1	3.34	0.289
2	11.1	3.37	0.275
2	30.8	3.43	0.237
2	55.5	3.48	0.191
6	0.6	3.36	0.299
6	3.1	3.43	0.292
6	11.1	3.46	0.28
6	30.8	3.51	0.246
6	55.5	3.58	0.198
10	0.6	3.39	0.301
10	3.1	3.46	0.294
10	11.1	3.5	0.28
10	30.8	3.54	0.249
10	55.5	3.57	0.204

When investigating the bubble size distributions (Figure 2 and Figure 3), no significant differences can be recognized neither with increasing countercurrent liquid flow, nor increasing gas flow rate. However slightly smaller bubbles are observed at the lowest countercurrent liquid flow and at the lowest gas flow rate.

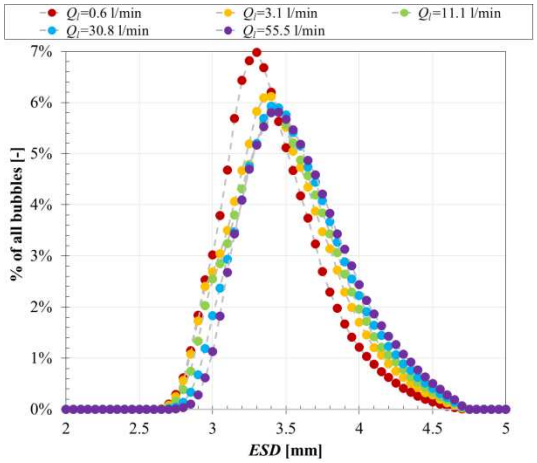

Figure 2. Bubble *ESD* distributions at different countercurrent liquid flow rates for Q_g=10 l/h air volume flow rate.

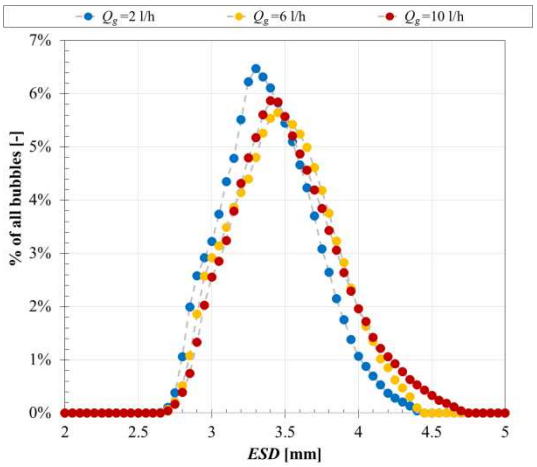

Figure 3. Bubble *ESD* distributions at different air volume flow rates for Q_l=11.1 l/min countercurrent liquid flow rate.

In contrast, considerable mean velocity changes of the bubbles at different countercurrent flow rates can be observed in the velocity distributions in Figure 4. With increasing countercurrent liquid flow, the bubble velocity distributions show similar aspects, but the peaks of the distributions are shifted towards lower velocities. Additionally, with an increasing gas flow rate, the position of the peaks of the bubble velocity distributions remains the same, but the distribution profiles become wider (Figure 5).

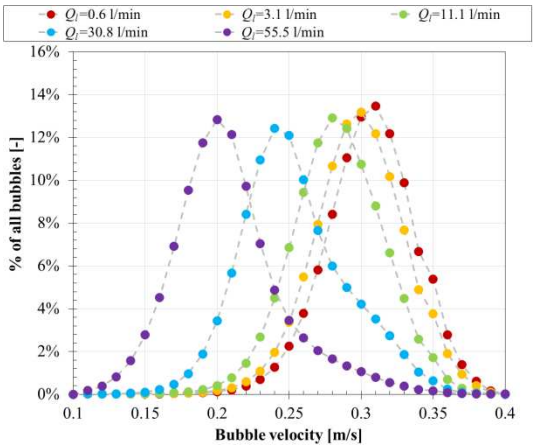

Figure 4. Bubble velocity distributions at different countercurrent liquid flow rates for Q_g=10 l/h air volume flow rate.

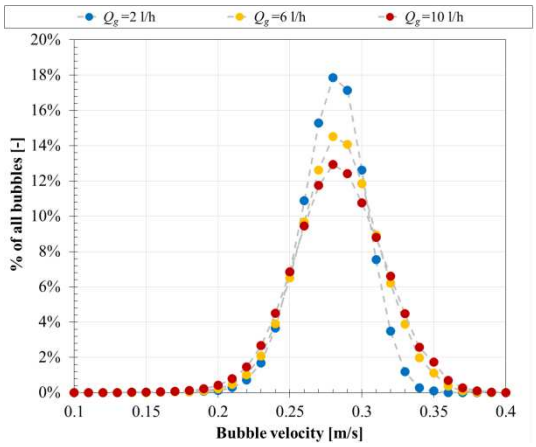

Figure 5. Bubble velocity distributions at different air volume flow rates for Q_l=11.1 l/min countercurrent liquid flow rate.

Liquid dynamics

After combining the results of all four measurement windows (obtained simultaneously with the four cameras) a full view of the liquid flow field within the column can be obtained (Figure 6).

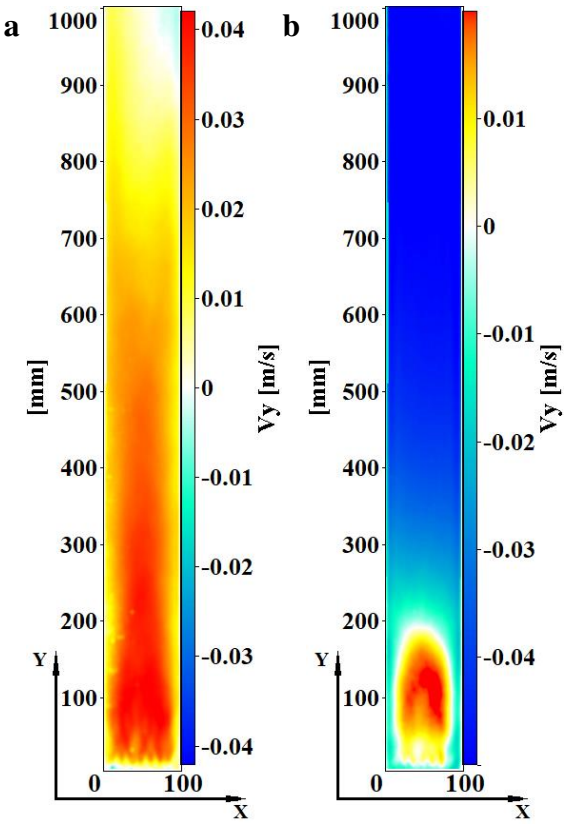

Figure 6. Mean vertical liquid velocity fields obtained from measurements with Q_g=10 l/h air flow rate for Q_l=0.6 l/min (a) and 30.8 l/min (b) countercurrent liquid flow. (Please mind the different colour scales: warm colours represent positive, cold colours negative flow directions).

As expected, the mean images show an almost symmetric vertical velocity field in the bubble column, where the rising bubbles generate an ascending flow in the centre of the column. This ascending flow is slowed down (Figure 6, a) and is stopped (Figure 6, b) by the countercurrent liquid flow. This phenomenon can be followed more clearly on the vertical velocity profiles, which are obtained in the centre of the bubble column (between 45 and 55 mm) for each investigated case (Figure 7 and Figure 8).

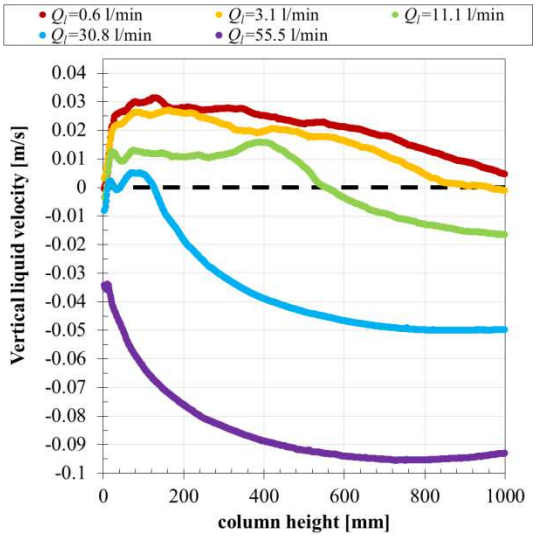

Figure 7. Vertical profiles of the mean vertical liquid velocity in the centre of the bubble column for all investigated countercurrent liquid flows at Q_g=6 l/h air flow rate.

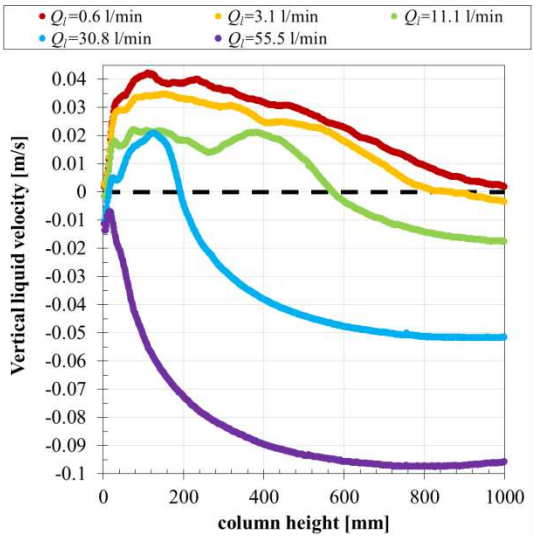

Figure 8. Vertical profiles of the mean vertical liquid velocity in the centre of the bubble column for all investigated countercurrent liquid flows at Q_g=10 l/h air flow rate.

At both investigated gas volume flow rates, 6 and 10 l/h, the vertical profiles show similar trends

at the same countercurrent liquid flow rate. However, due to the slightly larger bubbles and higher bubble velocities, higher vertical velocities are measured at higher gas volume flow rate (Figure 8). At the two lowest liquid flow rates, 0.6 and 3.1 l/min, the bubble generated ascending flow dominates the flow in the bubble column. Starting from the inlet nozzles up to around 100 mm the vertical liquid velocity increases and then it continuously decreases to the end of the investigated domain at 1000 mm. At 11.1 l/min countercurrent liquid flow the vertical velocity increases close to the inlet nozzles, but then it stagnates at around 400 mm. From this height, the vertical liquid velocity suddenly decreases and the flow changes its direction around 580 mm above the nozzles due to the higher countercurrent liquid flow. This point, where the direction of the flow changes, is shifted towards the nozzles with higher countercurrent liquid flow rates. The trend of the vertical velocity profiles at the highest countercurrent liquid flow rates, 30.8 and 55.5 l/min, are nearly the same from 400 mm upwards at both investigated gas flow rates. Below 400 mm, the influence of the different gas flow rates can be observed. As a result of the higher gas flow rate, higher vertical liquid velocities are obtained in this region.

If the measured bubble velocities and vertical liquid velocities are plotted together in one plot, it becomes obvious, that the liquid flow follows the same trend as the bubble velocities. As well as the liquid velocity, also the bubble velocity decreases continuously from 100 mm along the column height at lower countercurrent liquid flows (Figure 9). In these cases, the liquid flow is dominated by the bubbles. Similarly, at higher countercurrent liquid flows (Figure 10) the liquid velocity profiles follow the bubble velocity profiles. Here, the influence of the bubbles on the liquid flow is reduced with the increasing countercurrent liquid flow.

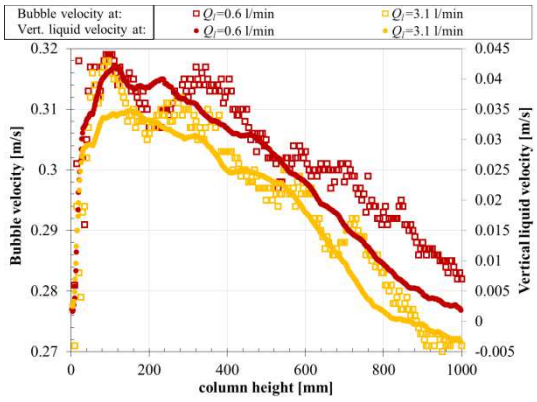

Figure 9. Vertical profiles of the mean vertical bubble velocity and the mean vertical liquid velocity in the centre of the bubble column for Q_l=0.6 and 3.1 l/min countercurrent liquid flows at Q_g=10 l/h air flow rate.

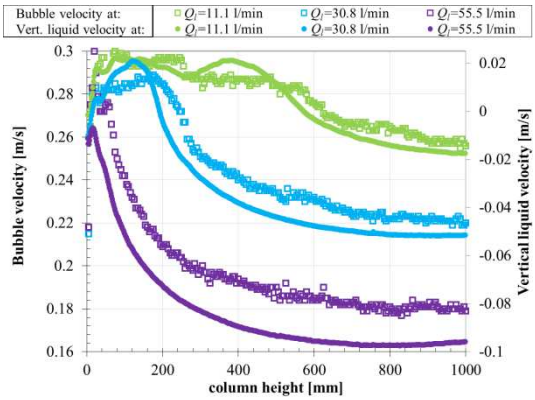

Figure 10. Vertical profiles of the mean vertical bubble velocity and the mean vertical liquid velocity in the centre of the bubble column for Q_l=11.1, 30.8 and 55.5 l/min countercurrent liquid flows at Q_g=10 l/h air flow rate.

From these results it is evident, that with increasing countercurrent flow the bubble velocity decreases, therefore the bubble residence time in the column increases, which is beneficial for mass transfer. From another point of view, in two-phase flows with mass transfer, besides a high residence time also a good mixing is demanded, which enhances mass transfer. Analysing the horizontal liquid velocities in the bubble column (Figure 11), it is noticeable that at the highest countercurrent liquid flow rates at 30.8 and 55.5 l/min, where the bubble residence time is the highest, horizontal velocity fluctuations can be found just in the first 1-200 mm above the inlet nozzles.

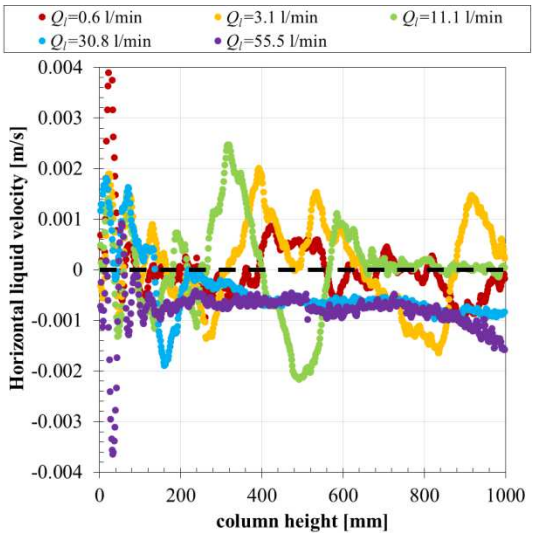

Figure 11. Vertical profiles of the mean horizontal liquid velocity in the centre of the bubble column for all investigated countercurrent liquid flows at Q_g=10 l/h air flow rate.

At lower countercurrent liquid flow rates, where the bubbles have larger effect on the liquid flow in the bubble column, much higher horizontal liquid velocities are measured. Supposedly the best mass transfer rate could be achieved at 11.1 l/min countercurrent liquid flow, where the bubble velocity is noticeably lower than in the cases with 0.6 and 3.1 l/min and remarkably horizontal liquid velocity fluctuations are measured.

Simulation results

For comparison between simulation and experiment, profiles are extracted at the upper edge of the observation region 1 m above the nozzles along the line in which these are arranged (x-direction). Since the flow is unsteady, the simulation data are averaged over a period of time, which has been determined to be sufficiently long to reproduce the expected mirror symmetry in the profiles to a good approximation. In addition, to match the experimental setup, the calculated values are averaged in the horizontal direction perpendicular to the line of the nozzles (y-direction) over a region corresponding to the depth-of-field of the camera used in the measurements.

An exemplary comparison between calculated and measured gas fraction profiles is shown in Figure 12 with the experimental conditions indicated in the caption. The experimental gas fraction here has been determined from the measured bubble trajectories by counting the frequency of occurrence of a bubble centre in cells of a 5 mm^3 grid and multiplying by the bubble volume.

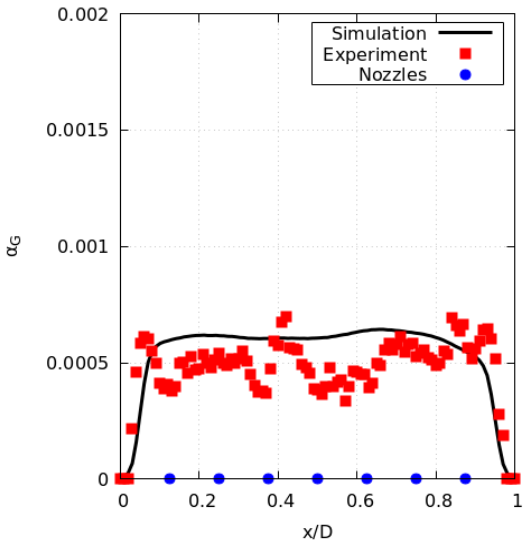

Figure 12. Comparison of calculated (line) and measured (symbols) gas fraction profiles for Q_l=0.6 m/s and Q_g=2 l/h. Bubbles had a mean size of d_b =3.8 mm.

As can be seen from the figure, the overall agreement between simulation and experiment is quite good. The average value in the central part of the column is slightly overpredicted by the simulations, but the drop near the column walls is captured very well. Some amount of fluctuations is visible in the measurements, which is likely due to unavoidable differences between the 7 nozzles resulting in somewhat uneven injection of gas. Such differences are of course absent in the simulations.

The result from the simulations for the liquid and gas velocities for the same flow conditions is shown in Figure 13. For this condition, the liquid flow was not measured so that a direct comparison to the experiment is not possible yet. A more comprehensive comparison for further observables and varied experimental conditions will be pursued in the near future.

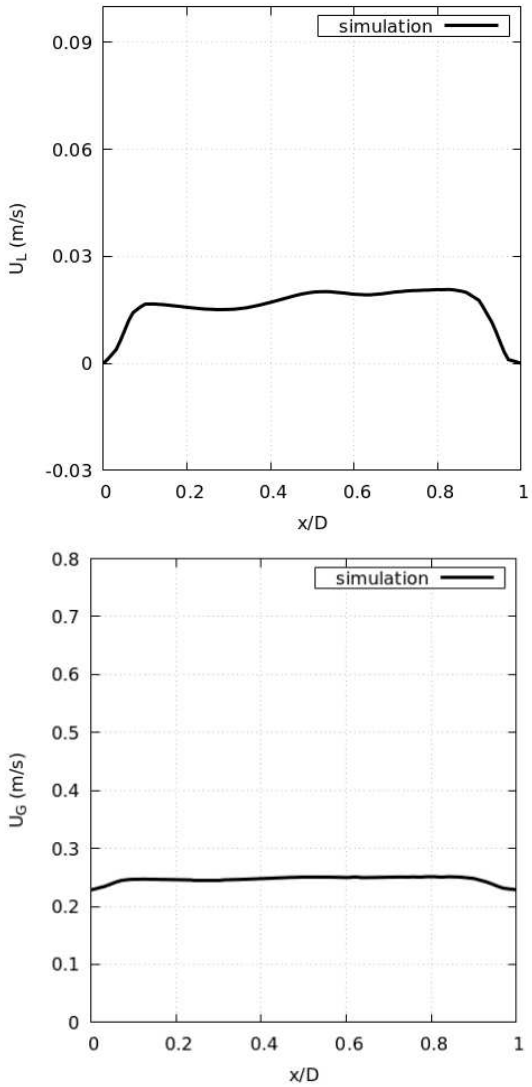

Figure 13. Simulated profiles for the liquid (top) and gas (bottom) velocities at Q_l=0.6 m/s and Q_g=2 l/h respectively.

5. CONCLUSIONS

In this paper two optical measurement techniques for characterizing the fluid dynamics of a countercurrent laboratory-scale bubble column reactor have been used. Shadow imaging combined with PTV was applied to obtain bubble parameters like bubble major and minor axis, and velocity, while the PIV technique was employed to characterize the liquid flow.

The analysis of the gathered bubble diameters has shown that no significant differences exist in the bubble size neither with increasing countercurrent liquid flow, nor with increasing gas flow rate. In contrast, as it was expected, the mean bubble velocity decreases continuously with increasing countercurrent liquid flow.

With the help of PIV, the flow field in the bubble reactor was investigated at different gas and countercurrent liquid flow rates. Combining the images of the four cameras, a full description of the hydrodynamics in the whole column was obtained. It has been found that at lower countercurrent liquid flows the flow is driven by the bubbles, while at higher countercurrent flow rates the ascending liquid flow, generated by the bubbles, is slowed down or close to the inlet nozzles even stopped. This phenomenon could considerably influence the mass transfer in the bubble column. For this reason, also mass transfer measurements are planned for the future in the bubble column.

Euler-Euler simulations according to the experimental setup were run using previously established closure models. A preliminary comparison between simulation results and measured data suggest, that these models are also applicable to the present case. This remains to be verified by a more detailed and comprehensive analysis which is still in progress.

ACKNOWLEDGEMENTS

Authors would like to thank the German Research Foundation (DFG) for the financial support under Grant No ZA 527/3-1 and RZ 11/3-1. We would also like to acknowledge the experimental support of our students Steffen Erichson and Maximilian Mahler. The workshop of LSS supported the set-up of the bubble column and measurement arrangement.

REFERENCES

[1] Joshi JB, Nandakumar K (2015), Computational Modeling of Multiphase Reactors. Annual Review of Chemical and Biomolecular Engineering 6:347-378

[2] Guo K, Wang T, Liu Y, Wang J (2017), CFD-PBM simulations of a bubble column with different liquid properties. Chem Eng J 329:116-127

[3] Besagni G, Guédon GR, Inzoli F (2018), Computational fluid-dynamic modeling of the mono-dispersed homogeneous flow regime in bubble columns. Nucl Eng Des 331:222-237

[4] Braga Vieira C, Litrico G, Askari E, Lemieux G, Proulx P (2018), Hydrodynamics of Bubble Columns: Turbulence and Population Balance Model. ChemEngineering 2:12

[5] Rzehak R, Krauss M, Kovats P, Zahringer K (2017), Fluid dynamics in a bubble column: New experiments and simulations. Int J Multiphase Flow 89:299-312

[6] Rzehak R, Ziegenhein T, Kriebitzsch S, Krepper E, Lucas D (2017), Unified modeling of bubbly flows in pipes, bubble columns, and airlift columns. Chem Eng Sci 157:147-158

[7] Shi P, Rzehak R (2018), Bubbly flow in stirred tanks: Euler-Euler/RANS modeling. Chem Eng Sci 190:419-435

[8] Kováts P, Thévenin D, Zähringer K (2018), Characterizing fluid dynamics in a bubble column aimed for the determination of reactive mass transfer. Heat Mass Transfer 54:453-461

[9] Kováts P (2021), Detailed experimental study of mass transfer and liquid flow in a bubble column with optical measurement techniques, Laboratory of Fluid Dynamics and Technical Flows.

[10] Menter FR (2009), Review of the shear-stress transport turbulence model experience from an industrial perspective. International Journal of Computational Fluid Dynamics 23:305-316

[11] Ma T, Santarelli C, Ziegenhein T, Lucas D, Fröhlich J (2017), Direct numerical simulation–based Reynolds-averaged closure for bubble-induced turbulence. Physical Review Fluids 2,

[12] Schlegel F, Draw M, Evdokimov I, et al. (2021), HZDR Multiphase Addon for OpenFOAM.

[13] Ishii MZ, N. (1979), Drag coefficient and relative velocity in bubbly, droplet or particulate flows. AlChE J 25:843-855

[14] Tomiyama A, Tamai H, Zun I, Hosokawa S (2002), Transverse migration of single bubbles in simple shear flows. Chem Eng Sci 57:1849-1858

[15] Hosokawa S, Tomiyama A, Misaki S, Hamada T (2002), Lateral Migration of Single Bubbles Due to the Presence of Wall.855-860

[16] Burns AD, Frank T, Hamill I, Shi JM, The Favre Averaged Drag Model for Turbulent Dispersion in Eulerian Multi-Phase Flows. In: 5th International Conference on Multiphase Flow, Yokohama, Japan, (2004).